Sains Malaysiana 47(9)(2018): 2035–2045
http://dx.doi.org/10.17576/jsm-2018-4709-11

The Effect of ZnO Loading for the Enhancement of PSF/ZnO-GO Mixed Matrix Membrane Performance

(Kesan Muatan ZnO untuk Peningkatan Prestasi PSF/ZnO-GO Campuran Matriks Membran)

NURUL 'ADILAH ROSNAN, TEOW YEIT HAAN* & ABDUL WAHAB MOHAMMAD

ABSTRACT

This study was aimed to investigate the effect of ZnO-decorated GO nanocomposite material loaded with different weight percent of ZnO toward polysulfone (PSF) mixed-matrix membrane (MMM) performance enhancement. ZnO-decorated GO nanocomposite material was loaded with 1, 5, 10 and 20 wt. % ZnO was blended with PSF polymer and fabricated through phase inversion process. The performance of the fabricated MMMs were evaluated by measuring membrane permeability, bovine serum albumin rejection (BSA) and flux recovery ratio (FRR). Experiment results demonstrated that the PSF/ZnO-GO MMM performances were greatly improved where 10 wt. % ZnO loaded into ZnO-decorated GO nanomaterial exhibited the highest permeability (5.35 L/m²·h·bar) and BSA retention at all pH state among all fabricated mixed-matrix membranes. Additionally, FRR was also dramatically improved attributed to the smoother membrane surface. This work has shown that a well distribution of ZnO with the help of GO nanosheet as a dispersing agent blended with PSF polymer to form PSF/ZnO-GO MMM was a promising approach in creating better ultrafiltration (UF) membrane with a better hydrophilicity, permeability, and cleaning efficiency for the used in food industry in future.

Keywords: Food processing; graphene oxide; mixed-matrix membrane; ultrafiltration; zinc oxide

ABSTRAK

Kajian ini bertujuan mengkaji kesan perbezaan peratus muatan ZnO pada komposit nano GO-ZnO terhadap peningkatan prestasi membran matrik-bercampur (MMM) polisulfon (PSF). Komposit nano GO-ZnO dimuatkan dengan 1, 5, 10, dan 20 % bt. ZnO kemudiannya diadun bersama polimer PSF dan dihasilkan melalui proses songsangan fasa. Prestasi MMM dinilai daripada segi kebolehtelapan, penolakan albumin serum bovin (BSA) dan nisbah pemulihan fluks (FRR). Keputusan kajian menunjukkan prestasi MMM PSF/GO-ZnO meningkat dengan 10 % bt. ZnO dimuatkan pada komposit nano GO-ZnO mempamerkan kebolehtelapan luar biasa (5.35 L/m²·h·bar) dengan penolakan BSA yang tinggi terhadap semua keadaan pH. Tambahan, FRR juga meningkat secara mendadak disebabkan permukaan membran yang lebih licin. Penemuan yang terdapat dalam kajian ini membuktikan keseragaman agihan ZnO dibantu oleh kepingan nano grafin oksida (GO) sebagai ejen penyebaran diadun bersama polimer PSF bagi menghasilkan MMM PSF/GO-ZnO merupakan pendekatan menjanjikan penghasilan membran ultra penurasan (UP) yang lebih baik dengan peningkatan hidrofilik, kebolehtelapan dan kecekapan pembersihan untuk digunakan dalam industri makanan pada masa akan datang.

Kata kunci: Grafin oksida; membran matrik-bercampur; pemprosesan makanan ultra penurasan; zink oksida

INTRODUCTION

Protein is recognized as one of the most essential ingredients in the food and pharmaceutical industries (Wen-qiong et al. 2017). Ultrafiltration (UF) membrane offers great potential to concentrate and fractionate protein products without the use of high temperature, addition of additives or preservatives which might change the properties of the food components. However, membrane fouling which resulted permeate flux decline was the major obstacle for wide application of membrane technology. This has driven the researches to study the technology to overcome the membrane fouling via incorporation of nanoparticles (NPs) into the membrane matrix for the fabrication of mixed-matrix membrane which has received the most attention (Ho et al. 2018).

Various types of metal oxide or metal NPs have been reported for the used in mixed-matrix membrane fabrication, including zirconium dioxide (ZrO_2) (Taghizadeh & Vatanparast 2016), iron (II) oxide (Fe_2O_3) (Gui et al. 2015), magnesium oxide (MgO) (Silva & Avillez 2016), aluminum oxide (Al_2O_3) (Peng et al. 2018), titanium dioxide (TiO_2) (Teow et al. 2015), silicon dioxide (SiO_2) (Wu et al. 2017), silver (Ag) (Mahmoudi et al. 2015) and zinc oxide (ZnO) (Leo et al. 2012). For example, Teow et al. (2015) studied the addition of 0.01 g/L TiO_2 nanoparticles into polyvinylidene fluoride (PVDF) mixed-matrix membrane exhibited excellent permeability and rejection of humid acid.

Among all NPs, ZnO was the most effective additive used for membrane fabrication as it was inexpensive,

presenting superb properties in antimicrobial and having high thermal and mechanical stability (Rajabi et al. 2015). The fabricated mixed matrix membrane (MMM) with the incorporation of ZnO NPs has proven in successfully improved the membrane performance by depicting higher porosity, permeability, rejection, hydrophilicity and enhanced antifouling property (Chung et al. 2016).

Although it was proven could enhance the membrane performance, aggregation of ZnO NPs still a drawback for this fouling propensity development in membrane fabrication process (Shen et al. 2012). Attributed to this, graphene oxide (GO) nanosheet was introduced as a reliable platform for better nanomaterials dispersion (Layek & Nandi 2013). The functional groups on GO nanosheet were act as anchor sites in forming hybrid nanostructure with ZnO NPs (Wang et al. 2014). Through these interactions, the integration of both ZnO NPs and GO nanosheet would form nanohybrid with homogeneous dispersion of ZnO NPs for the enhancement of membrane performance. However, there is a lack of study on ZnO loading in ZnO-decorated GO nanocomposite material for the enhancement of MMM performance. Hence, the objective of this study was to investigate the effect of ZnO weight percent loaded into GO nanosheet towards membrane performance enhancement.

Materials and Methods

Materials

Graphite powder, zinc acetate dehydrates ($Zn(CH_3COO)_2{\cdot}2H_2O$), oxalic acid ($C_2H_2O_4{\cdot}2H_2O$), sodium nitrate ($NaNO_3$) and N-methyl-2-pyrrolidine (NMP) were purchased from Merck Co., Germany. 98% sulfuric acid (H_2SO_4), 38% hydrochloric acid (HCl), 30% hydrogen peroxide (H_2O_2), absolute ethanol and potassium permanganate ($KMnO_4$) were supplied by Sigma Aldrich, USA. Polysulfone (PSF) pallet was obtained from Goodfellow Cambridge Ltd., England. All chemicals used were in analytical grade.

Synthesis of GO

Graphene oxide (GO) was synthesized from graphite powder followed the modify Hummers' method as described in previous study (Mahmoudi et al. 2015). The synthesized GO was freeze dried under vacuum to obtain brown powder product for further study.

Synthesis of ZnO-decorated GO Nanocomposite Material

GO suspension was prepared by dispersing 0.3 g of GO in 10 mL of absolute ethanol under sonication using an ultrasonicator, WUC-A03H (Wisd. Korea) with frequency of 40 KHz. 0.01 to 0.20 g of $Zn(CH_3COO)_2{\cdot}2H_2O$ was added into 90 mL of absolute ethanol under vigorous stirring at 65°C for 30 min. Next, GO suspension was added into $Zn(CH_3COO)_2{\cdot}2H_2O$ and absolute ethanol mixture and stirred for 20 min at 45°C. Finally, 1 g of $C_2H_2O_4{\cdot}2H_2O$ dissolved in 50 mL absolute alcohol was added into the mixture and kept stirring for another 90 min. The precipitate was collected by centrifugation and dried overnight in an oven at 65°C. The resulted product was calcined at 400°C for 3 h to produce ZnO-decorated GO nanocomposite material. ZnO-decorated GO nanocomposite materials loaded with different weight percent of ZnO (1, 5, 10 and 20 wt. %) were obtained by manipulating the quantity of $Zn(CH_3COO)_2{\cdot}2H_2O$ used during the synthesis process.

Characterization of Nanomaterials
X-ray Diffraction (XRD)

The crystal phase of synthesized nanomaterials was analyzed using D8 Advance X-ray diffractometer (Bruker AXS, Germany) equipped with CuKα radiation source (1.5406 Å) at 2θ scan range of 5° to 85°.

Fourier Transform Infrared Spectroscopy (FTIR)

FTIR spectrum was recorded by Nicolet 6700 FTIR spectrometer (Thermo Fisher Scientific Inc., USA) to identify the possible functional group and chemical bonding of GO nanosheet. The FTIR spectrum was obtained from 32 scans with 4 cm^{-1} resolution and operated at wavelength ranging from 4000 to 500 cm^{-1}.

Field Emission Scanning Electron Microscopy (FESEM) and Energy Dispersive X-ray Spectroscopy (EDX)

High resolution FESEM, Gemini model SUPRA 55VP (Calr Zeiss, Germany) was used to examine the morphology and structure of GO nanosheet and ZnO-decorated GO nanocomposite material. All samples were coated with a thin layer of platinum under vacuum to reduce the surface charge on the samples so that contrastive image can be observed under the electron microscope. In a meantime, the element compositions on the samples were identified using EDX, Oxford INCA PentaFETX3 (Oxford, UK).

Fabrication of Membrane

Neat PSF membrane and PSF/ZnO-GO MMM were fabricated through phase inversion technique using NMP as solvent and ultrapure (UP) water as non-solvent bath. First, 0.6 wt. % of ZnO-decorated GO nanocomposite material was added into NMP and sonicated at the frequency of 40 kHz for 30 min. Next, 20 wt. % of PSF was dissolved into the ZnO-decorated GO nanocomposite material and NMP mixture and continuously stirred at 250 rpm and 60 ± 5°C for 5 h to form a homogeneous solution (Chung et al. 2017). The resulted membrane polymer solution was casted onto a clean glass plate using Filmographe Doctor Blade 360099003 (Braive Instrumen, Germany) at the thickness of 0.2 mm. Subsequently, the glass plate with the membrane polymer solution was horizontally immersed into the UP water bath at room temperature for a day to ensure the complete

solidification and the removal of residual solvent (Teow et al. 2015). Different formulation of PSF/ZnO-GO MMMs were summarized in Table 1.

Characterization of Membrane

Membrane Morphology

Membranes topology and cross-section were examined using high resolution FESEM as described in before in characterization of nanomaterials section. For membrane cross-section observation, the membrane sample was cyro-fractured into appropriate-size by immersing it into liquid nitrogen before mounted on the sample holder. The outer surface of the membrane sample was coated with a thin layer of platinum using the sputter coating chamber before examined under electron microscope at an accelerating voltage of 3 kV. In a meantime, the zinc element distributed on the membrane surface was analyzed using EDX mapping analysis.

Atomic Force Microscopy (AFM)

Membrane surface roughness was characterized using AFM NTEGRA Prime (NT-MDT, Russia) at semi-contact mode under ambient conditions. The scanned area was 5 5 μm using the laser beam, reflected by cantilevers tip situated above the membrane sample's surface. A three-dimensional image was then generated.

Porosity and Mean Pore Radius

Membrane porosity (ε) is the percentage of void space in a membrane. It was determined by gravimetric method, calculated using (1):

$$\varepsilon = \frac{\omega_1 - \omega_2}{A \times n \times d_w} \quad (1)$$

where ω_1 is the weight of the wet membrane (g); ω_2 is the weight of the dry membrane (g); A is the membrane effective area (m^2); n is the membrane thickness (m); and d_w is the water density (998 kg/m^3). While the membrane mean pore radius (r_m) was estimated from the porosity data using Guerout-Elford-Ferry equation:

$$r_m = \sqrt{\frac{(2.9 - 1.75\varepsilon)\, 8\eta l Q}{\varepsilon \times A \times \Delta P}} \quad (2)$$

where ε is the membrane porosity (%); ŋ is the water viscosity (8.9 10^{-4} Pa.s); l is the membrane thickness (m); Q is the permeated volume per unit time (m^3/s); A is the membrane effective area (m^2); and ΔP is the applied pressure (Pa).

Contact Angle

Contact angle meter, Model FM40Mk2 (Kruss GmbH, Germany) with Drop Shape Analysis Software was used to measure the static contact angle on the membrane surface which indicates the membrane hydrophilicity. The contact angle was measured at 3 different spots on the membrane surface to minimize the analytical errors.

Performance Evaluation of the Synthesized Membranes

Membrane Permeability

Membrane permeability was evaluated using the dead-end membrane filtration unit. UP water was employed as the feed for membrane compaction and for the evaluation of membrane permeability. Prior the membrane permeability test, the membrane was pressurized at constant pressure of 8 bar for 1 h to reduce the impact of membrane compaction during the filtration process. Then, the membrane permeation flux was measured at different operating pressure of 1, 2, 3 and 4 bar. Data of permeate flux against pressure was plotted and the membrane permeability was obtained from the gradient of the linear line. The membrane permeation flux was calculated using the following equation:

$$J = \left(\frac{V}{At}\right) \quad (3)$$

where V is the permeate volume (L); A is the membrane effective area (m^2); and t is the operating time (h).

TABLE 1. Formulation of the synthesized membranes

Membrane	PSF (wt. %)	NMP (wt. %)	Weight percent of ZnO-decorated GO (wt. %)	Weight percent of ZnO loading (wt. %)
Neat PSF	20	80	0.6	0
PSF/ZnO-GO MMM, 1 wt. % ZnO	20	80	0.6	1
PSF/ZnO-GO MMM, 5 wt. % ZnO	20	80	0.6	5
PSF/ZnO-GO MMM, 10 wt. % ZnO	20	80	0.6	10
PSF/ZnO-GO MMM, 20 wt. % ZnO	20	80	0.6	20

BSA REJECTION

1 g/L of BSA solution at different pH value (pH 4, 7 and 8) was used as the feed solution for BSA rejection. 300 mL of BSA solution was initially added into the dead-end stirred cell. BSA rejection study was conducted at constant pressure of 4 bar and at stirring speed of 200 rpm. The membrane rejection was calculated using the following equation:

$$R = (1 - \frac{C_p}{C_f}) \times 100\% \quad (4)$$

where C_p is the concentration of the permeate (mg/mL) and C_f is the concentration of the feed solution (mg/mL).

FLUX RECOVERY RATIO (FRR)

Membrane antifouling property was evaluated based on its ability to recover to its original pure water flux after hydraulic cleaning process. The membrane after used for 2 h of BSA rejection test was taken out from the base of dead-end stirred cell. It was rinsed and soaks in UP water for 1 h. Following, the membrane pure water flux after the hydraulic cleaning process was tested using UP water as the feed. FRR was calculated using the following equation:

$$FRR = \left(\frac{J_2}{J_1}\right) \times 100\% \quad (5)$$

where J_1 is the pure water flux ($L/m^2 \cdot h$) before the rejection test; and J_2 is the pure water flux ($L/m^2 \cdot h$) after the hydraulic cleaning.

RESULTS AND DISCUSSION

CHARACTERIZATION OF GO NANOSHEET AND ZNO-DECORATED GO NANOCOMPOSITE MATERIAL

The XRD pattern of graphite, GO nanosheet and ZnO-decorated GO nanocomposite material loaded with 20 wt. % of ZnO are presented in figures (Figure 1). Pristine graphite depicted a strong peak at 26.5° and it was shifted to 10.8° for GO nanosheet, indicated the success exfoliation of graphite into GO nanosheet. Followed by the decoration of GO nanosheet with ZnO NPs, the characteristic peak of GO nanosheet at $2\theta = 10.8°$ was disappeared. Paulchamy et al. (2015) reported that the diffraction peak of GO nanosheet would be reduced or even vanished if the regular stacks of GO nanosheet or graphite were destroyed by exfoliation (Paulchamy et al. 2015). However, XRD pattern of ZnO-decorated GO nanocomposite material showed some broad peaks in the range of 15° to 80°, which were assigned by the ZnO NPs decorated on GO nanosheet (Mathialagan et al. 2017).

The existence of C=O and C-OOH functional groups on GO nanosheet was further verified by FTIR spectra as shown in Figure 2. The characteristic peak at 1627.4 cm^{-1} was assigned by C=O stretching vibration whereas the broad peak around 3586.1 cm^{-1} was correspond to the hydroxyl (O-H) stretching vibration. In addition, two bands at 1070.4 and 1417.3 cm^{-1} were attributed by C-OOH and alkoxy (R-O) groups, respectively. The existence of the aforementioned functional groups proved the successful oxidation of graphite to GO nanosheet where similar results had been presented by other researchers (Ho et al. 2017).

The morphology and structure of GO nanosheet and ZnO-decorated GO nanocomposite material were characterized using FESEM, while EDX analysis was used to examine the elemental compositions existed on both nanomaterials. As could be seen from Figure 3(a) at 100 k× of magnification, GO nanosheet was appeared as a thin film. The decoration of GO nanosheet with ZnO NPs added the white dots in FESEM micrograph of ZnO-decorated GO nanocomposite material was further confirmed by EDX analysis. As depicted in Figure 3(b), the element compositions attributed by ZnO-decorated GO nanocomposite material was presenting an additional element, zinc as compared to GO nanosheet which confirmed the existence of ZnO NPs onto GO nanosheet.

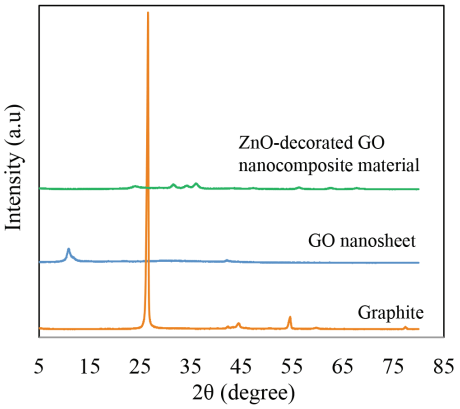

FIGURE 1. XRD pattern of graphite, GO nanosheet and ZnO-decorated GO nanocomposite material loaded with 20 wt. % ZnO

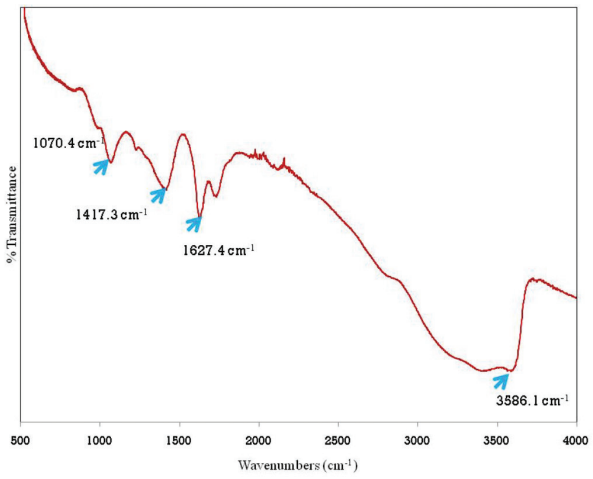

FIGURE 2. FTIR spectra of GO naosheet

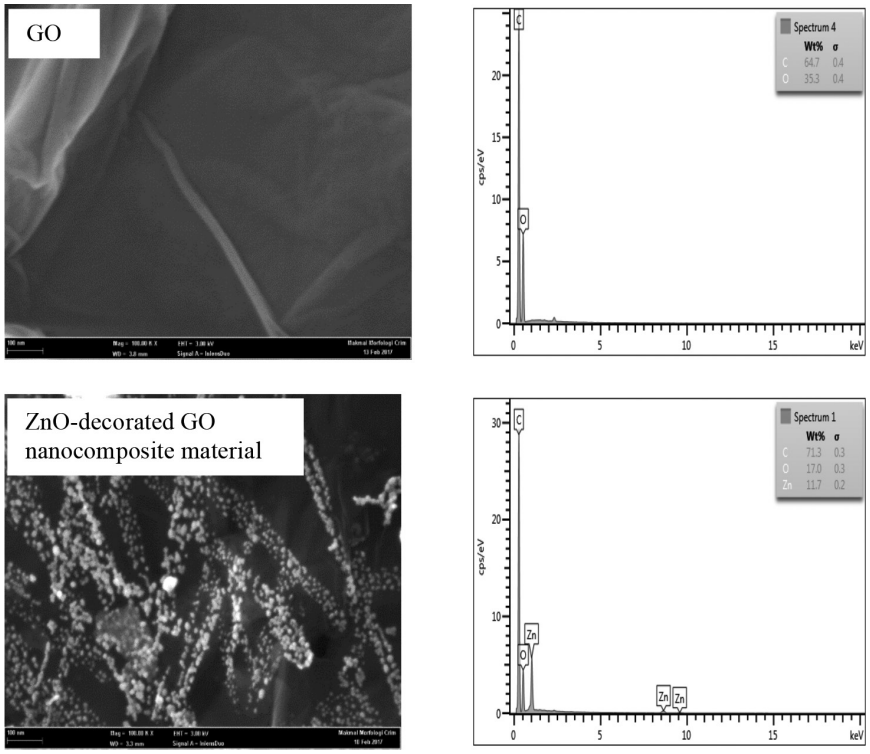

(a) (b)

FIGURE 3. (a) FESEM micrographs and (b) EDX spectra of GO nanosheet and ZnO-decorated GO nanocomposite material loaded with 20 wt. % ZnO

CHARACTERIZATION OF MEMBRANE

MORPHOLOGY AND STRUCTURE

FESEM micrographs of the membrane surface shown in Figure 4(a) indicates that the neat PSF membrane showed less pores on the membrane surface as compared to PSF MMM incorporated with ZnO-decorated GO nanocomposite material. On the other hand, cross-section micrographs of the fabricated membranes showed that all membranes have typical asymmetric and highly porous structure with a dense skin layer which responsible for permeation and rejection, followed by finger-like structure and sponge-like layer. However, neat PSF membrane possessed a thicker sponge-like layer and dense skin layer. This was possibly due to the delayed de-mixing rate between solvent and non-solvent which slower the phase inversion process compared to the fabrication process of MMM (Chung et al. 2017). Strong hydrophilic property of ZnO-decorated GO nanocomposite material has the tendency to attract more water towards the MMM during the phase inversion process, thus resulted in faster de-mixing rate and creating more porous network (Rabiee et al. 2015).

Figure 4(c) shows the zinc element distribution on the fabricated membranes. The zinc element was non-detectable on neat PSF membrane surface. However, it was existed on the surface of MMM showed by green dots on the EDX map. The zinc element exhibited well and homogeneous dispersion on PSF/ZnO-GO MMMs. Unfortunately, a crowd of green dots were seen at the mapping image for PSF/ZnO-GO MMM loaded with 20 wt. % of ZnO, where agglomeration of ZnO NPs might have happened.

SURFACE ROUGHNESS

Figure 5 presents the three-dimensional AFM images of the fabricated membranes with different weight percent of ZnO loaded into ZnO-decorated GO nanocomposite material. Whereas Table 2 quantitatively summarized the average surface roughness of the fabricated membranes. As shown in Figure 5(a), neat PSF membrane surface was covered with 'valley-like peaks'. Hence, it is not surprise that PSF membrane was having the highest average surface roughness value among all other membranes. Less sharp peaks or valleys were noticed on three-dimensional AFM images of PSF/ZnO-GO MMMs depicted by Figure 5(b), 5(c), 5(d) and 5(e). The results was contradicting to the study conducted by Padaki et al. (2015) where the increasing of nanomaterial concentration had showed an increment on membrane surface roughness. Smoother PSF/ZnO-GO MMMs' surface than neat PSF membrane was possibly attributed by the ZnO-decorated GO nanocomposite material had occupied the ridge-valley structure of the membrane thus leads to smoother membrane surface. Hence, the incorporation of ZnO-decorated GO nanocomposite material into the membrane

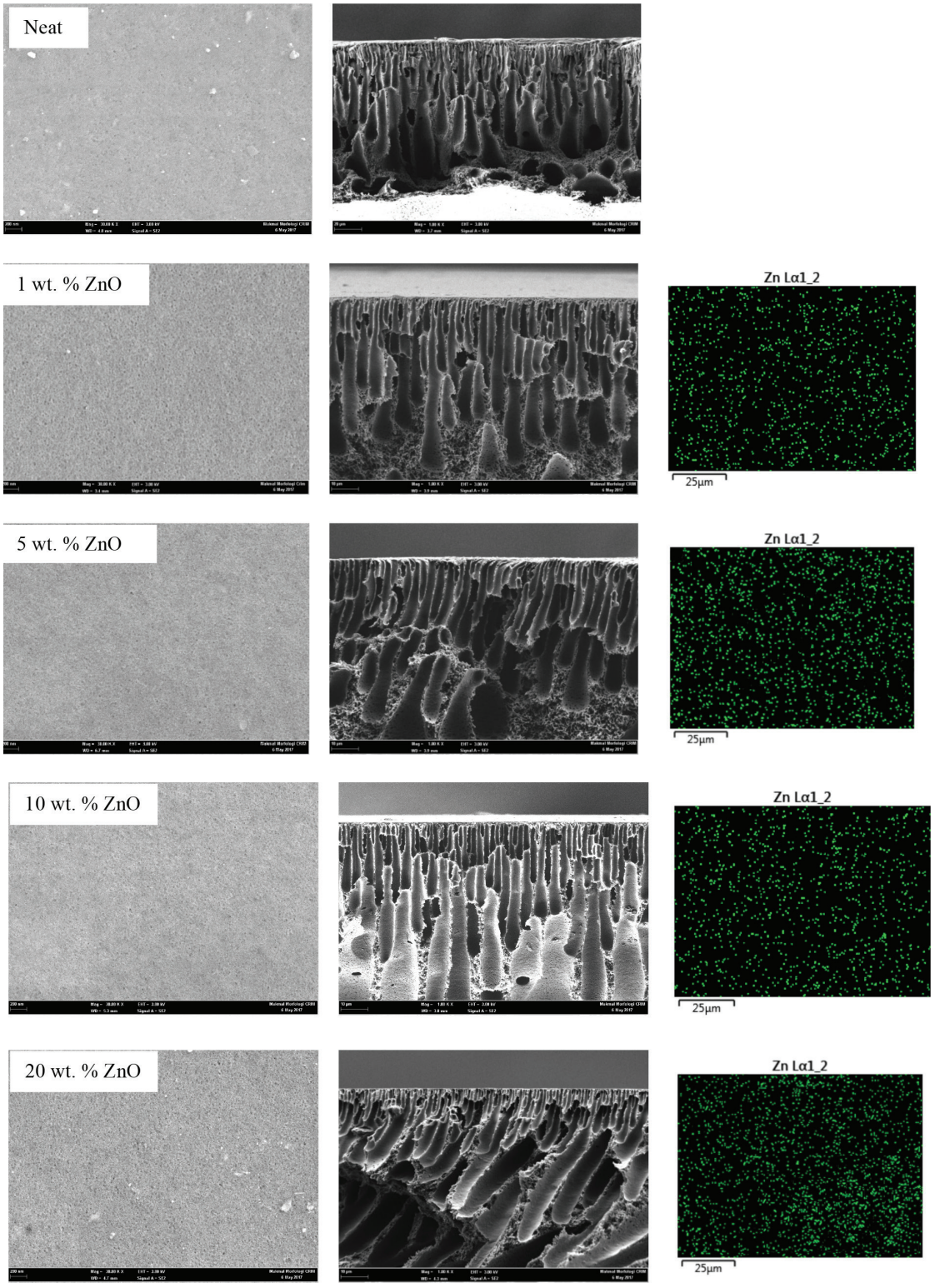

FIGURE 4. FESEM micrographs of (a) membrane topology (b) membrane cross-section, and (c) EDX mapping for zinc element distribution on the membrane surface

matrix which contributing to a smoother membrane surface was expected to enhance the membrane anti-fouling property.

POROSITY AND MEAN PORE RADIUS

Porosity and mean pore radius of the fabricated membranes at different weight percent of ZnO loaded into ZnO-

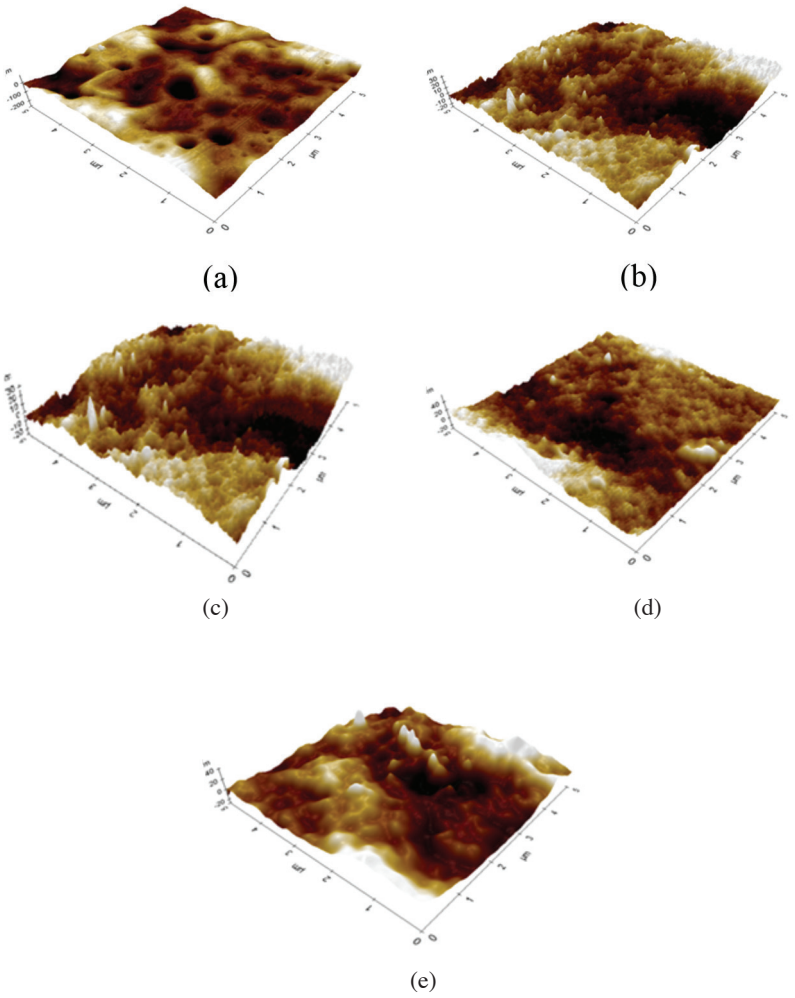

FIGURE 5. AFM images of (a) Neat PSF membrane, PSF/ZnO-GO MMM with (b) 1 wt. % ZnO loading (c) 5 wt. % ZnO loading (d) 10 wt. % ZnO loading, and (e) 20 wt. % ZnO loading

TABLE 2. Average surface roughness of the fabricated membranes

Membrane	Average surface roughness, R_a (nm)
Neat PSF	21.30 ± 1.25
PSF/ZnO-GO MMM, 1 wt. % ZnO	6.50 ± 0.55
PSF/ZnO-GO MMM, 5 wt. % ZnO	6.70 ± 0.62
PSF/ZnO-GO MMM, 10 wt. % ZnO	6.00 ± 0.71
PSF/ZnO-GO MMM, 20 wt. % ZnO	7.50 ± 0.93

decorated GO nanocomposite material were summarized in Table 3. As shown in Table 3, the porosity of the membrane was increased by increasing the weight percent of ZnO loaded into ZnO-decorated GO nanocomposite material. This phenomenon was commonly seen in the fabrication of mixed-matrix membrane such as Vun et al. (2017) were noted that greater membrane porosity and pore size was depicted on mixed-matrix membrane with increase concentration of Fe_3O_4-GO loaded into the membrane matrix (Vun et al. 2017). The enhancement

TABLE 3. Porosity and mean pore radius of the fabricated membranes

Membrane	Porosity, ε (%)	Mean pore radius, r (nm)
Neat PSF	78.14 ± 1.71	5.37 ± 0.21
PSF/ZnO-GO MMM, 1 wt. % ZnO	84.23 ± 0.86	7.87 ± 0.10
PSF/ZnO-GO MMM, 5 wt. % ZnO	87.97 ± 0.33	13.58 ± 0.04
PSF/ZnO-GO MMM, 10 wt. % ZnO	90.61 ± 0.71	14.65 ± 0.07
PSF/ZnO-GO MMM, 20 wt. % ZnO	89.95 ± 0.76	13.08 ± 0.08

hydrophilicity of membrane polymer solution attributed by the hydrophilic functional groups appeared on ZnO-decorated GO nanocomposite material would accelerate the membrane formation process by speeding up the de-mixing rate between solvent and non-solvent, thus increased the membrane porosity and mean pore radius (Ho et al. 2017; Rabiee et al. 2015).

However, the membrane porosity was slightly decreased at highest ZnO loading of 20 wt. %. High concentration of ZnO loaded into ZnO-decorated GO nanocomposite material led to an increase in membrane polymer solution viscosity, which hinder the exchange between solvent and non-solvent during phase-inversion and slow down the solidification of the membrane. Consequently, the formation of macro-voids was suppressed and less porous membrane was formed. Coincide to the increasing of membrane porosity with the increasing of ZnO weight percent loaded into ZnO-decorated GO nanocomposite material, membrane mean pore radius was also enlarged from 5.37 to 14.64 nm with the increasing of ZnO loading up to 10 wt. %. Similar to the analysis result obtained for membrane porosity, membrane mean pore radius was decreased as ZnO loading was further increased to 20 wt. %.

WETTABILITY

Contact angle analysis is an indicator for membrane wettability. Figure 6 shows the contact angle of the fabricated membranes at different weight percent of ZnO loaded into ZnO-decorated GO nanocomposite material. Neat PSF membrane was exhibited the highest contact angle of 77.29°. The contact angle value was then reduced to 75.08°, 65.23°, 63.93° and 66.95° with the ZnO loading of 1, 5, 10 and 20 wt. %, respectively. The decrement in membrane contact angle value with the incorporation of ZnO-decorated GO nanocomposite material was possibly due to the existence of abundance hydrophilic groups of ZnO-decorated GO nanocomposite material which has high affinity towards water (Sun et al. 2015). However, the contact angle value was increased as ZnO loading was increased to 20 wt. %. The oppose effect could be related to the agglomeration of ZnO-decorated GO nanocomposite material which eventually lead to surface inhomogeneity and slightly higher average surface roughness (Zambare et al. 2017). The same observation was found in a research conducted by Padaki et al. (2015). Hence, the water droplet was not able to spread on the rough membrane surface covered with peaks or valleys.

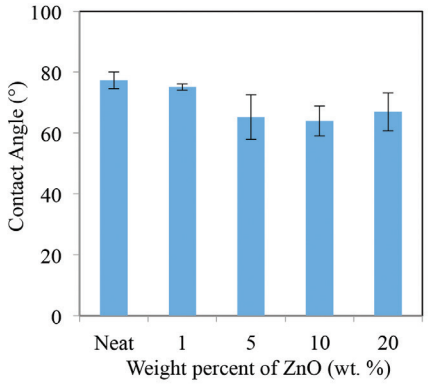

FIGURE 6. Contact angle of the fabricated membranes

PERFORMANCE EVALUATION OF THE MEMBRANES

MEMBRANE PERMEABILITY

Figure 7 depicts the permeability of the fabricated membranes at different weight percent of ZnO loaded into ZnO-decorated GO nanocomposite material. As shown in Figure 7, the membrane permeability was increased from 0.35 to 5.35 L/m^2·h·bar for ZnO loading up to 10 wt. % and slightly decreased to 3.85 L/m^2·h·bar at highest ZnO loading of 20 wt. %, correlated to the membrane contact angle results. This phenomenon might be due to increasing wettability of MMM with the deposition of ZnO-decorated GO nanocomposite material into the membrane matrix (Subasi & Cicek 2017). The improved membrane wettability could be explained by the polar ZnO NPs and functional groups on the surface of GO nanosheet have high affinity towards water molecules which could attract more water molecules to pass through the membrane (Kumar et al. 2016).

Besides, higher permeability of MMM can be explained by its porosity and mean pore radius. The increasing membrane permeability of MMM was attributed by enhanced porosity and larger mean pore radius compared to neat PSF membrane as tabulated in Table 3. It was in good agreement with Zinadini et al. (2017) finding where the inclusion of ZnO-decorated GO nanocomposite material has resulted in higher porosity and mean pore radius of MMM, which eventually enhanced the permeability of the membrane (Zinadini et al. 2017). However, higher weight percent of ZnO loaded into ZnO-decorated GO nanocomposite material causing the irregular positioning of ZnO-decorated GO nanocomposite material in the membrane matrix and blocked the membrane pores. Therefore, it decreased the membrane hydrophilicity, membrane porosity and mean pore radius. The combination of these changes in membrane matrix has attributed to a slight decrement in membrane permeability for PSF/ZnO-GO MMM incorporated with ZnO-decorated GO nanocomposite material of 20 wt. % ZnO loading.

BSA REJECTION TEST

As shown in Figure 8, all fabricated membranes were successfully rejecting more than 90% of BSA from the feed solution despite the pH of the feed solution. The increment of ZnO loaded into ZnO-decorated GO nanocomposite material has enhanced the performance of PSF/ZnO-GO

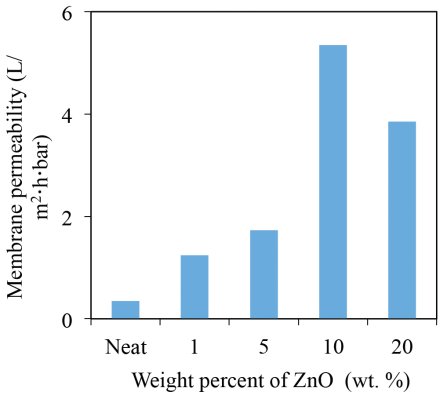

FIGURE 7. Permeability of the fabricated membranes

MMM towards BSA rejection where the maximum BSA rejection was achieved by PSF membrane incorporated with ZnO-decorated GO nanocomposite material loaded with 10 wt. % ZnO. According to Rabiee et al. (2015), BSA has higher affinity towards hydrophobic surface rather than hydrophilic surface. Therefore, the increasing of BSA rejection by MMM was possibly due to the increased hydrophilicity of MMM and prevents BSA adsorption. However, 20 wt. % of ZnO loaded into ZnO-decorated GO nanocomposite material was excessive. It leads to the agglomeration of ZnO-decorated GO nanocomposite material thus increased the hydrophobicity of the membrane and reduced its performance.

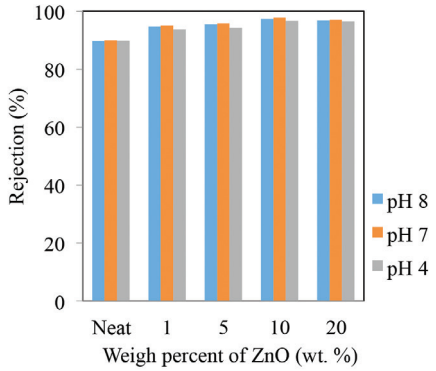

FIGURE 8. Performance of the fabricated membranes

Meanwhile, the lowest BSA rejection was observed for the feed solution at pH4. In particular, pH was found to be an important parameter influencing the protein aggregation. The isoelectric point of the protein is in the range pH5.5-8. The net surface charge of the protein is minimum at this pH range and easily aggregates (Luo et al. 2016). Therefore, it could be easily remove through the sieving effect attributed by the membrane pores. However, less aggregation of protein occurred in BSA solution at pH4 where the protein was more soluble and has high possibility to pass through the membrane pores, thus contributing to lower BSA rejection.

FLUX RECOVERY RATIO (FRR)

Higher FRR ratio indicates that the used membrane was having higher ability to recover to its original pure water flux after the hydraulic cleaning. It reflects that the membrane has indirectly depicted higher fouling resistance with lower level of persistent protein adsorption onto the membrane surface. Figure 9 displays that neat PSF membrane was only able to recover 58.33% to 63.89% of water flux, which was the lowest compared to PSF/ZnO-GO MMMs. Low recovery of the pure water flux was possibly due to higher surface roughness of neat PSF membrane compared to PSF/ZnO GO MMMs and promoted the accumulation of BSA molecules that were difficult to remove even with hydraulic cleaning. Whereas, smoother surface of PSF/ZnO-GO MMMs remarkably improved the membrane cleaning efficiency where the water will roll off the protein or accumulated foulant away from the membrane surface during hydraulic cleaning.

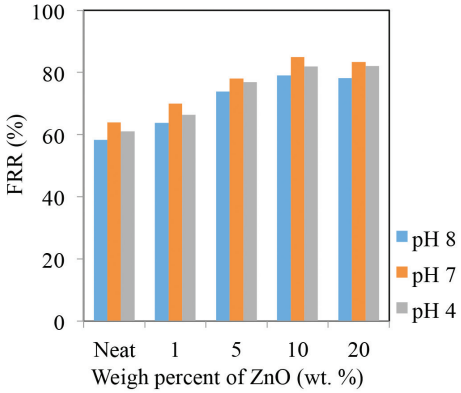

FIGURE 9. FRR of the fabricated membranes

CONCLUSION

The effect of ZnO loaded into ZnO-decorated GO nanocomposite material for the performance of PSF/ZnO-GO MMM was investigated in this study. The best performance membrane was dedicated to PSF membrane blended with 10 wt. % ZnO loaded into ZnO-decorated GO nanocomposite material. The increasing of ZnO weight percent loaded into the ZnO-decorated GO nanocomposite material up to 10 wt. % led to a maximum in membrane permeability, 5.35 L/m²·h·bar. This mainly due to the higher surface wettability and more pore structure created on PSF/ZnO-GO MMM loaded with 10 wt. % of ZnO. Besides, PSF/ZnO-GO MMM loaded with 10 wt. % of ZnO has achieved BSA rejection up to 98% regardless the pH value of the feed solution. The effect of ZnO loaded into ZnO-decorated GO nanocomposite material resulted in increased hydrophilicity of MMM, thus prevent BSA adsorption. Additionally, it was also shown an enhanced ability to recover to initial pure water flux after the hydraulic cleaning of used membrane where FRR for PSF/ZnO-GO MMM loaded with 10 wt. % of ZnO was up to 85% regardless the pH value of the

feed solution. The FRR improved dramatically could be attributed to the smoother surface of the membrane which improved the membrane cleaning efficiency. Hence, this work has shown that a well distribution of ZnO with the help of GO nanosheet as a dispersing agent blended with PSF polymer to form PSF/ZnO-GO MMM was a promising approach in creating better UF membrane with a better hydrophilicity, permeability, and cleaning efficiency for the used in food industry in future.

ACKNOWLEDGEMENTS

The authors appreciate the financial support by Geran Universiti Penyelidikan (GUP-2017-098) and Dana Penyelidikan Strategik (KRA-2017-016).

REFERENCES

Chung, Y.T., Mahmoudi, E., Mohammad, A.W., Abdelbaki, B., Daniel, J. & Nidal, H. 2017. Development of polysulfone-nanohybrid membranes using ZnO-GO composite for enhanced antifouling and antibacterial control. *Desalination* 402: 123-132.

Chung, Y.T., Ba-Abbad, M.M., Mohammad, A.W. & Benamor, A. 2016. Functionalization of zinc oxide (ZnO) nanoparticles and its effects on polysulfone-Zno membranes. *Desalination and Water Treatment* 57(17): 7801-7811.

Gui, M., Papp, J.K., Colburn, A.S., Meeks, N.D., Weaver, B., Wilf, I. & Bhattacharyya, D. 2015. Engineered iron/iron oxide functionalized membranes for selenium and other toxic metal removal from power plant scrubber water. *Journal of Membrane Science* 488: 79-91.

Ho, K.C., Teow, Y.H., Mohammad, A.W., Ang, W.L. & Lee, P.H. 2018. Development of graphene oxide (GO)/multi-walled carbon nanotubes (MWCNTs) nanocomposite conductive membranes for electrically enhanced fouling mitigation. *Journal of Membrane Science* 552: 189-201.

Ho, K.C., Teow, Y.H., Ang, W.L. & Mohammad, A.W. 2017. Novel GO/OMWCNTs mixed-matrix membrane with enhanced antifouling property for palm oil mill effluent treatment. *Separation and Purification Technology* 177: 337-49.

Kumar, M., Zahra, G., Anne, M.K.N., Mathias, U. & Jenny, L. 2016. Preparation and characterization of low fouling novel hybrid ultrafiltration membranes based on the blends of GO-TiO_2 nanocomposite and polysulfone for humic acid removal. *Journal of Membrane Science* 506: 38-49.

Layek, R.K. & Nandi, A.K. 2013. A review on synthesis and properties of polymer functionalized graphene. *Polymer* 54: 5087-5103.

Leo, C.P., Lee, C.W.P., Ahmad, A.L. & Mohammad, A.W. 2012. Polysulfone membranes blended with ZnO nanoparticles for reducing fouling by oleic acid. *Separation and Purification Technology* 89: 51-56.

Luo, X., Vasiljevic, T. & Ramchandran, L. 2016. Effect of adjusted pH prior to ultrafiltration of skim milk on membrane performance and physical functionality of milk protein concentrate. *Journal of Dairy Science* 99(2): 1083-1094.

Mahmoudi, E., Law, Y.N., Muneer, M.B.A. & Mohammad, A.W. 2015. Novel nanohybrid polysulfone membrane embedded with silver nanoparticles on graphene oxide nanoplates. *Chemical Engineering Journal* 277: 1-10.

Mathialagan, S., Ponnaiah, G.P. & Vijay, M. 2017. Synthesis and characterization of GO-ZnO nanocomposite material exhibiting photo catalytic degradation of dye waste water. *Journal of Scientific & Industrial Research* 76: 44-49.

Padaki, M., Emadzadeh, D., Masturra, T. & Ismail, A.F. 2015. Antifouling properties of novel PSF and TNT composite membrane and study of effect of the flow direction on membrane washing. *Desalination* 362: 141-150.

Paulchamy, B., Arthi, G. & Lignesh, B.D. 2015. A simple approach to stepwise synthesis of graphene oxide nanomaterial. *Journal of Nanomedicine & Nanotechnology* 6: 253-256.

Peng, D., Chen, J., Jiao, L. & Liu, Y. 2018. A fast-responding semi-transparent pressure-sensitive paint based on through-hole anodized aluminum oxide membrane. *Sensors and Actuators A: Physical* 274: 10-18.

Rabiee, H., Vahid, V., Mohammad, H.D.A.F. & Hamed, Z. 2015. Improvement in flux and antifouling properties of PVC ultrafiltration membranes by incorporation of zinc oxide (ZnO) nanoparticles. *Separation and Purification Technology* 156(Part 2): 299-310.

Rajabi, H., Ghaemi, N., Madaeni, S.S., Daraei, P., Astinchap, B., Zinadini, S. & Razavizadeh, S.H. 2015. Nano-ZnO embedded mixed matrix polyethersulfone (PES) membrane: Influence of nanofiller shape on characterization and fouling resistance. *Applied Surface Science* 349: 66-77.

Shen, L., Bian, X., Lu, X., Shi, L., Liu, Z., Chen, L., Hou, Z. & Fan, K. 2012. Preparation and characterization of ZnO/polyethersulfone (PES) hybrid membranes. *Desalination* 293: 21-29.

Silva, L. & Avillez, R.R.D. 2016. Sintering and characterization of magnesium oxide macroporous membranes. *Ceramics International* 42(2B): 3317-3321.

Subasi, Y. & Bugra, C. 2017. Recent advances in hydrophilic modification of PVDF ultrafiltration membranes-A review: Part II. *Membrane Technology* 11: 5-11.

Sun, X., Jing, Q., Peng-Fei, X., Bei-Bei, G., Chun-Miao, Y., Chao, S. & Shu-Guang, W. 2015. Graphene oxide-silver nanoparticle membrane for biofouling control and water purification. *Chemical Engineering Journal* 281: 53-59.

Taghizadeh, M.T. & Vatanparast, M. 2016. Ultrasonic-assisted synthesis of ZrO_2 nanoparticles and their application to improve the chemical stability of nafion membrane in proton exchange membrane (PEM) fuel cells. *Journal of Colloid and Interface Science* 483: 1-10.

Teow, Y.H., Ahmad, A.L., Lim, J.K., Ngang, H.P., Ling, Y.S. & Ooi, B.S. 2015. Hydroxyl functionalized PVDF-TiO_2 ultrafiltration membrane and its antifouling properties. *Journal of Applied Polymer Science* 132(21): 1-11.

Vun, C.P., Mohammad, A.W., Haan, T.W. & Mahmoudi, E. 2017. Evaluation of iron oxide decorated on graphene oxide (FE3O4/GO) nanohybrid incorporated in PSF membrane at different molar ratios for congo red rejection. *Jurnal Teknologi* 79(1-2): 73-81.

Wang, Y-W., Aoneng, C., Yu, J., Xin, Z., Jia-Hui, L., Yuanfang, L. & Haifang, W. 2014. Superior antibacterial activity of zinc oxide/graphene oxide composites originating from high zinc concentration localized around bacteria. *ACS Applied Materials & Interfaces* 6(4): 2791-2798.

Wu, H., Huang, J. & Liu, Y. 2017. Polysulfone ultrafiltration membrane incorporated with Ag-SiO_2 nanohybrid for effective fouling control. *Journal of Water and Health* 15(3): 341-352.

Zambare, R.S., Dhopte, K.B., Patwardhan, A.V. & Nemade, P.R. 2017. Polyamine functionalized graphene oxide polysulfone mixed matrix membranes with improved hydrophilicity and anti-fouling properties. *Desalination* 403: 24-35.

Zinadini, S., Saeed, R., Vahid, V. & Elham, J. 2017. Preparation of antibiofouling polyethersulfone mixed matrix NF membrane using photocatalytic activity of ZnO/MWCNTs nanocomposite. *Journal of Membrane Science* 529: 133-141.

Teow Yeit Haan* & Abdul Wahab Mohammad
Research Centre for Sustainable Process Technology
Faculty of Engineering and Built Environment
43600 UKM Bangi, Selangor Darul Ehsan
Malaysia

Nurul 'Adilah Rosnan, Teow Yeit Haan*&
Abdul Wahab Mohammad
Chemical Engineering Program
Faculty of Engineering and Built Environment
Universiti Kebangsaan Malaysia
43600 UKM Bangi, Selangor Darul Ehsan
Malaysia

*Corresponding author; email: yh_teow@ukm.edu.my

Received: 29 March 2018
Accepted: 14 May 2018